 FDMP, vol.2, no.4, pp.247-260, 2006

Modeling of Dendritic Growth in Alloy Solidification with Melt Convection

C.P. Hong[1], M.F. Zhu[2] and S.Y. Lee[1]

Abstract: In typical solidification processes the flow of molten metal is usually regarded as an unavoidable phenomenon potentially affecting the morphology of dendritic growth. Fundamental understanding of such flow is thus important for predicting and controlling solidification microstructures. This paper presents numerical simulations on the evolution of dendritic microstructures with melt convection. A two-dimensional modified cellular automaton (MCA) coupled with a transport model is developed to simulate solidification of binary and ternary alloys in the presence of fluid flow. This model takes into account the effects of the constitutional undercooling and curvature undercooling on the equilibrium interface temperature. It also considers the preferred growth orientation of crystals and solute redistribution during solidification. The flow dynamics and mass transport both by convection and diffusion are numerically solved using a SIMPLE scheme. The physics of the complete time-dependent interaction among melt convection, mass transfer and dendritic growth is naturally included in the model.

keyword: Cellular automaton, Convection, Deflection behavior, Dendritic growth, Side-branching.

1 Introduction

Dendritic growth, which is considered to be controlled by the complex interplay of thermal, solutal, capillary, crystallographic anisotropy, thermodynamics and physical properties, is commonly observed in normal solidification of alloys. The evolution of dendritic microstructures is strongly affected either by natural or forced convection since convection may alter the local heat and solutal transfer at the solid/liquid interface during solidification [Schraga(1999)].

It was found from theoretical predictions and experimental observations that convective motion in liquid affects the diffusion fields and the kinetics of dendritic growth, leading to the formation of completely different dendritic patterns in comparison to pure diffusion controlled cases [Saville and Beaghton(1988), Lee and Chen(1995)]. Recently, a variety of convective effects potential affecting the microstructure of an alloy was reviewed by Lappa(2005) together with a critical discussion of possible related numerical approaches. A review on the effect of convection on generic solidification problems was also made by Amberg and Shiomi(2005). However, the effect of convection on dendritic growth during solidification has not yet been fully understood.

Numerical simulations have been attempted to investigate microstructure evolution in solidification with melt convection by phase field models [Tong, Beckermann, Karma and Li(2001), Jeong, Dantzig and Goldenfeld(2003), Natsume, Ohsasa and Narita(2002), Lan and Shih (2004)], and other numerical techniques, such as the front tracking method [Al-Rawahi and Tryggvason(2002), Lijian and Zabaras(2006)] and the sharp-interface method [Udaykumar, Marella and Krishnan(2003)], etc. The models were employed to study nonlinear and fully coupled convection and solidification on a microscopic scale. The simulations reproduce asymmetrical dendritic growth morphology, such as the deflection behavior of dendritic growth and the side-branching enhanced in the upstream direction, but hindered in the downstream direction. However, the above numerical activities have been limited to free dendritic growth with convection in cases of pure materials or binary alloys.

The models based on the cellular automaton (CA) technique can reproduce most of microstructural features in solidification of alloys observed experimentally with an acceptable computational efficiency[Nastac(1999), Belteran-Sanchez and Stefanescu (2004)], indicating an excellent potential for engineering applications. Shin and Hong(2002) developed a cellular automaton model to study the effect of convection on dendritic growth

[1] Dept. of Metallurgical Eng.,Yonsei University, Seoul, Korea, e-mail: hong@yonsei.ac.kr

[2] Dept. of Materials Science and Eng., Southeast University, Nanjing, China.

morphology of Al-Cu alloys. This model is based on the coupling of a cellular automaton algorithm for dendritic growth and a continuum diffuse interface model as known from the phase field methodology, for solving the species and momentum transfer with convection.

Recently, a novel simulation approach based on a two-dimensional modified cellular automaton (MCA) coupled with a transport model was developed to study dendritic growth by the present authors [Zhu and Hong (2001)]. The MCA model was extended to simulate dendritic growth behavior under melt convection for a single equiaxed dendritic growth in a binary alloy system [Zhu, Lee and Hong(2004), Zhu, Dai, Lee and Hong(2005)]. In the classical CA models, since the growth velocity of dendritic grains is determined by the local undercooling based on a calculated thermal field, they can only provide grain structures, i.e., thermal dendritic grains, but dendritic growth features cannot be predicted. On the other hand, the MCA models account not only for a thermal field, but also for solute concentration and fluid flow fields during solidification. In addition, they also account for the effect of curvature on the interface temperature. Thus, the MCA models can provide dendritic growth features (solutal dendrites), microsegregation patterns, and other microstructural growth features such as eutectic growth and the formation of second phases [Zhu and Hong(2002)&(2004)].

In the present study, the previous MCA model was extended to multi-component alloy system via coupling with a thermodynamic and phase equilibrium calculation engine, PanEngine [Chen, Daniel, Zhang, Chang, Yan, Xie, Schmid-Fetzer and Oates(2002)]. The MCA model was applied to simulate the effect of fluid flow both on a single equiaxed dendritic growth in Al-rich binary and on columnar and equiaxed multi-dendritic growth in Al-rich ternary alloys. This paper also includes a brief review of our previous work on the modeling of dendritic growth with melt convection in a binary alloy system.

2 Mathematical model and formulation

2.1 Model Description

The MCA model for dendritic growth is coupled with a transport model for calculating solute transfer by both convection and diffusion during solidification. The two dimensional computational domain is divided into a uniform orthogonal arrangement of cells. Each cell is characterized by several variables, such as temperature, solute concentration (two solutes for ternary alloys), crystallographic orientation, solid fraction, pressure, flow vector, etc., and marked as the state of liquid ($f_s = 0$), solid ($f_s = 1$) or interface. Eight neighbor cells, including the four nearest neighbor cells and the four second-nearest neighbor cells, are taken into consideration to determine the interface cells. The interface cell must satisfy the condition that at least one of its eight neighbors is solid. ($0 \leq f_s < 1$). Since nucleation is not addressed in the present work, at the beginning of simulation several isolated crystal seeds with different preferential growth orientations are randomly assigned in the domain which is initially at a homogeneous temperature and composition. The seeds are given an index indicating their preferred crystallographic orientations of θ_0 with respect to the horizontal direction. Since the emphasis of the present study is on the solutally driven dendritic growth with a forced flow, the temperature field inside the domain is considered to be uniform with a constant thermal undercooling. The undercooled melt, assumed as an incompressible Newtonian fluid with an inlet flow velocity denoted as U_{in}, flows past the growing dendrites in the domain. The solidified dendrite is assumed to be rigid and stationary. As the dendrite grows into the undercooled and flowing melt, the geometry of the solid/liquid boundary changes, which in turn triggers an increasing complex fluid flow.

2.2 MCA approach for dendritic growth

Two of the key parameters needed in the modeling of dendritic growth in solidification of alloys are the solute partition coefficient and the liquidus slope. For a simple binary alloy system, they are usually considered to be constant. However, for multi-component systems, the assumption of the constant partition coefficient and liquidus slope is unlikely to be appropriate since the actual values may vary significantly with temperature and compositions. Accordingly, it is necessary to couple thermodynamic and phase equilibrium calculations in modeling of dendritic growth in multi-component alloy systems.

In the present study, in order to simulate dendritic growth for ternary alloys the MCA approach which was used in the previous studies [Zhu, Lee and Hong(2004), Zhu, Dai, Lee and Hong(2005)] was extended by coupling with the multi-component phase equilibrium calculation engine, PanEngine, which provides the phase equilib-

rium information of a ternary alloy system.

The growth of a dendrite is driven by the local undercooling, which consists of three contributions, i.e., thermal, solutal and curvature effects. Thus, the total undercooling at a dendrite tip is given by

$$\Delta T = \Delta T_T + \Delta T_C + \Delta T_R \tag{1}$$

where ΔT_T, ΔT_C and ΔT_R are the undercooling contributions associated with the thermal, the solutal, and the curvature effects, respectively. The thermal undercooling is assumed to be constant, while the solutal and curvature undercoolings depend upon the local concentration and the mean curvature at the solid/liquid interface. According to the local thermodynamic equilibrium at the solid/liquid interface, the local undercooling at time t_n, $\Delta T(t_n)$, is calculated from the difference between the local equilibrium liquidus temperature and the local actual temperature, incorporating with the effect of curvature, and is given by

$$\Delta T(t_n) = T^*(t_n) - T(t_n) - \Gamma(\theta)\overline{K}(t_n) \tag{2}$$

where $T^*(t_n)$ is the local equilibrium liquidus temperature, $T(t_n)$ is the local actual temperature, and $\Gamma(\theta)$ is the Gibbs-Thomson coefficient. For binary alloys the local equilibrium liquidus temperature is calculated by $T^*(t_n) = T_m + mC(t_n)$, here T_m is the equilibrium melting point of a pure material, m is the liquidus slope, and $C(t_n)$ is the local liquid composition. For ternary alloys, $T^*(t_n)$ is calculated with the aid of PanEngine according to the local liquid compositions of the two solutes. In the present work, the local actual temperature $T(t_n)$ is considered to be constant. The calculation of the interface mean curvature $\overline{K}(t_n)$ can be found elsewhere [Shin and Hong(2002)].

The normal interface growth velocity V_g and the local undercooling are related by the classical sharp interface model [Wheeler, Boettinger and McFadden(1992), Kim, Kim and Suzuki(1999)].

$$V_g = \mu_k \cdot \Delta T(t_n) \tag{3}$$

where μ_k is the interface kinetics coefficient.

It is well known that dendrites grow into specific crystallographic orientations. In modeling dendritic growth, it is therefore necessary to consider the anisotropy in either the surface energy or the interfacial attachment kinetics or both [Murray, Wheeler and Glicksman(1995)]. The present model accounts for the anisotropy in both the surface energy and interfacial kinetics. The interface kinetics coefficient$\mu_k$and the Gibbs-Thomson coefficient Γ are given by [Shin and Hong(2002)].

The growth velocities of the interface cells can be calculated using Eq.(2)$\sim$(3). Other detailed description can be found in the literature [Zhu and Hong(2004)].

2.3 Momentum and species transfer

In solidification of alloys under convection the solute redistribution during solidification is affected by fluid flow. The continuity and Navier-Stokes equations are written as follows:

Equation of continuity :

$$\nabla \cdot (\overrightarrow{u}) = 0 \tag{4}$$

Navier-Stokes equation :

$$\rho \frac{\partial(\vec{u})}{\partial t} + \rho(\overrightarrow{u}) \cdot \nabla(\overrightarrow{u}) = -\nabla P + \nabla \cdot (\mu \nabla(\overrightarrow{u}) \tag{5}$$

where $\overrightarrow{u}$ is the velocity vector, ρ is the density which is considered to be identical and constant in both liquid and solid phases, μ is the viscosity, and P is the hydrostatic pressure.

To describe phase transformations in a ternary alloy system, two solute fields are need to be calculated. The governing equation for species transfer in ternary alloy system in the presence of fluid flow is given by

$$\frac{\partial C_i(m)}{\partial t} + \left(\xi \vec{u}\right) \cdot \nabla C_i(m) = D_i(m)\nabla^2 C_i(m) + C_i(1-k)\frac{\partial f_s}{\partial t} \quad (i = s, l \text{ and } m = 1, 2) \tag{6}$$

where $C_i(m)$and $D_i(m)$ is the concentration and the diffusion coefficient of the solute element m in phase i(solid or liquid), and k is the partition coefficient. Two diffusion coefficients$D_i(m)$ are considered to be independent of composition, but temperature dependent. Two solutes are considered to diffuse independently each other and cross diffusion is neglected. Within the interface region, the solid and liquid phases are assumed to be in equilibrium and thus solute diffusion between the liquid and solid phases is ignored. ξ is a parameter which is dependent on the state of a cell: $\xi = 1$ ($f_s < 1$) and $\xi = 0$ ($f_s = 1$). It is obvious that the species transfer in solid is purely controlled by diffusion ($\xi = 0$).

Table 1 : Physical properties used in the present simulation [Zhu and Hong(2001), Shin and Hong(2002), Yan, Chen, Xie and Chang(2002), Ode, Lee,Kim Kim and Suzuki(2000)]

Definition	Symbol(units)	Value
Partition coefficient	k	0.1
Liquidus slope	m_l /K·(wt%)$^{-1}$	-3.36
Solute diffusion coefficient in liquid (binary)	D_l / m^2·s^{-1}	3.0×10^{-9}
Solute diffusion coefficient in solid (binary)	D_s / m^2·s^{-1}	3.0×10^{-13}
Liquid diffusion coefficient of Cu (ternary)	$D_l(Cu)$/ m^2·s^{-1}	$1.05\times10^{-7}\exp(-2856/T)$
Solid diffusion coefficient of Cu (ternary)	$D_s(Cu)$/ m^2·s^{-1}	$2.9\times10^{-5}\exp(-15600/T)$
Liquid diffusion coefficient of Mg (ternary)	$D_l(Mg)$/ m^2·s^{-1}	$9.9\times10^{-5}\exp(-8610/T)$
Solid diffusion coefficient of Mg (ternary)	$D_s(Mg)$/ m^2·s^{-1}	$0.37\times10^{-4}\exp(-14854/T)$
Average interface kinetics coefficient	$\overline{\mu}_k$ / m·(s·K)$^{-1}$	0.002
Average Gibbs-Thomson coefficient	$\overline{\Gamma}$ / m·K	1.7×10^{-7}
Viscosity	μ / P	0.014
Density	ρ / kg·m^{-3}	2.475×10^{3}

It is assumed that the local thermodynamic equilibrium is maintained at the solid/liquid interface and thus the solidified cells always adopt the equilibrium solid composition. As a dendrite grows, the growing cells reject solutes at the solid/liquid interface. The rejected amount of solute element m at one interval of time step is evaluated by

$$\Delta C(m) = \Delta f_s \left(C_l^*(m) - C_s^*(m)\right) \tag{7}$$

where Δf_s is the solid fraction increment of the interface cell at one interval of time step. $C_l^*(m)$ and $C_s^*(m)$ are the interface liquid and solid compositions of the solute element m, respectively. The interface solid composition $C_s^*(m)$ in Eq. (7) and the interface equilibrium liquidus temperature $T^*(t_n)$ in Eq. (2) are obtained with the aid of PanEngine according to the local interface liquid compositions of the two solutes $C_l^*(1)$ and $C_l^*(2)$, which are determined by numerically solving Eqs. (4)∼(6).

In order to simulate the incompressible fluid flow across the fixed and growing dendrites and the solute redistribution during solidification, which is controlled by both diffusion and convection, we employed a fully coupled solving scheme. The SIMPLE algorithm [Patankar(1980), Hong(2004)] based on the staggered grids was applied to solve the continuity and Navier-Stokes equations, Eqs.(4) and (5). Based on the calculated fluid flow field, the species transfer governing equation, Eq. (6), was solved using an implicit finite volume method and the tridiagonal matrix algorithm (TDMA)[Thomas(1949)]. Both the convection and diffusion terms were evaluated by the hybrid scheme for the pressure-velocity coupling in the momentum equations. The zero-flux boundary condition was imposed for mass transfer on the four outer boundaries of the calculation domain.

The coupled mechanism of a complete time-dependent interaction of melt convection, mass transfer and dendritic growth is directly embedded in the present model. The accuracy of the numerical scheme used in the present study was validated by the previous study[Zhu, Cao, Chen, Hong, and Chang(2006), Zhu, Hong, Stefanescu, and Chang(2006)].

The physical parameters used in the present simulation are listed in Table 1.

3 Results and discussion

3.1 Free dendritic growth of binary alloys

3.1.1 The effect of flow on dendritic growth behavior with various preferred growth orientations

In order to simulate the effect of flow on dendritic growth behavior with various preferred growth orientations, a two dimensional calculation domain was divided into

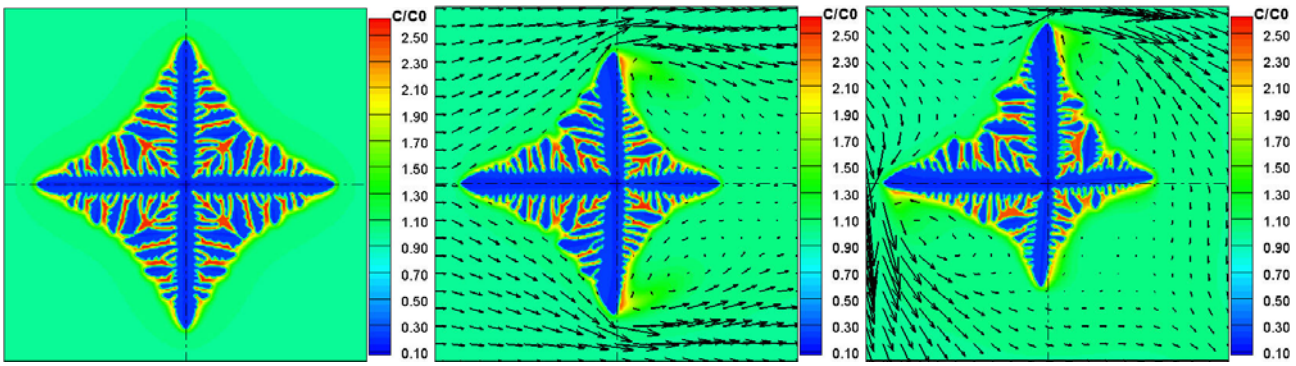

Figure 1 : Simulated dendritic growth morphology of an Al-2wt%Cu alloy solidified in an undercooled melt($\Delta T = 10.5K$) with a preferred growth orientation of $\theta_0 = 0^0$under various flow directions: (a) no flow(P_e=0), (b) horizontal flow(P_e=0.162) and (c) flow from 45^0($P_e(x) = P_e(y)$=0.115).

201×201 cells with a cell size of 0.5 μm. A seed crystal was assumed to locate at the center of the calculation domain. In the present study, binary Al-Cu and ternary Al-Cu-Mg alloys were adopted in order to compare the simulations with other theoretical and experimental studies reported in the literatures. The kinetic anisotropy coefficientδ_k and the surface energy anisotropy coefficient δ_t were chosen to be 0.3.

Figure 1 shows the simulated dendritic growth morphology and the solute profiles of an Al-2wt%Cu alloy solidified in an undercooled melt($\Delta T = 10.5K$) with a preferred growth orientation of $0^0$for various flow directions. The flow velocity is indicated by $P_e = 0.162$ for case (b) and $P_e(x) = P_e(y)$=0.115 for case (c). The vector plots illustrate the actual flow intensity and direction. For a clearer visualization, the velocity vectors are represented by 10 times coarser than those used in the calculation, i. e., every 10×10 cells show one flow vector.

In cases of phase field simulations, it is necessary to impose some artificial noise for the formation of sidebranches in dendritic growth. In addition, the amplitude of the sidebranches depends on the noise strength [Tong, Beckermann, Karma and Li(2001)]. However, in the present MCA model, sidebranching can be predicted without imposing any artificial noise in simulation [Zhu and Hong(2001)].

In case of a pure diffusion circumstance, case (a), a symmetric dendrite shape and solute distribution pattern were obtained. However, the symmetric dendrite shape and solute field are destroyed by fluid flow, as shown in cases (b) and (c), indicating that the growth of the dendrite arms and the side-branching are all promoted on the upstream side and inhibited on the downstream side. Comparing Fig.1 (b) with (a), the deflection behavior of the perpendicular arms can be found. The growth of solutal dendrites is known to be controlled by the transport of solutes from the growing solid/liquid interface into the supersaturated melt [Koss, LaCombe, Tennenhouse, Glicksman and Winsa(1999)]. It is evident that in the presence of convection, solute is washed away by fluid flow from the upstream to the downstream region, resulting in the asymmetrical solute profile in liquid, i.e., the concentration in the upstream region is lower than that in the downstream region.

For a hypoeutectic alloy, higher concentration at the solid/liquid interface yields larger negative local solutal undercooling and thereby lower dendritic growth velocity. As a consequence, the growth of the dendrite arms and the side-branching are all promoted in the upstream region and restrained in the downstream region, leading to asymmetrical dendrite morphology.

Figures 2 and 3 indicate the simulated dendritic growth morphology and the solute profiles of an Al-2wt%Cu alloy solidified in an undercooled melt($\Delta T = 10.5K$) for various flow directions, with a preferred growth orientation of 45^0 and 65^0, respectively.

It can be noted that the dendrite morphology is significantly influenced not only by the flow direction, but also by the preferred growth orientation. Dendritic growth is always enhanced in the upstream direction facing against the incoming flow and inhibited in the downstream direction.

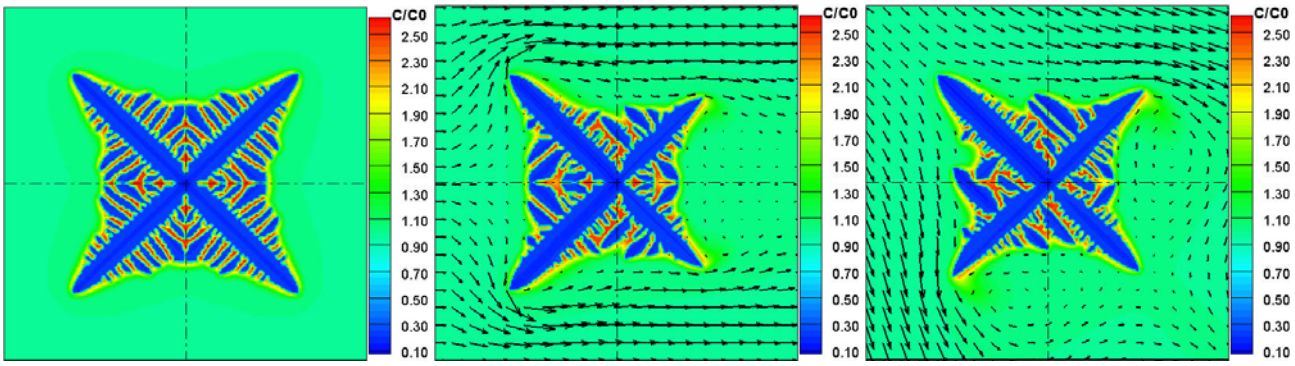

(a) (b) (c)

Figure 2 : Simulated dendritic growth morphology of an Al-2wt%Cu alloy solidified in an undercooled melt ($\Delta T = 10.5K$) with a preferred growth orientation of $\theta_0 = 45^0$ under various flow directions: (a) no flow(P_e=0), (b) horizontal flow (P_e=0.162) and (c) flow from 45^0($P_e(x) = P_e(y)$=0.115).

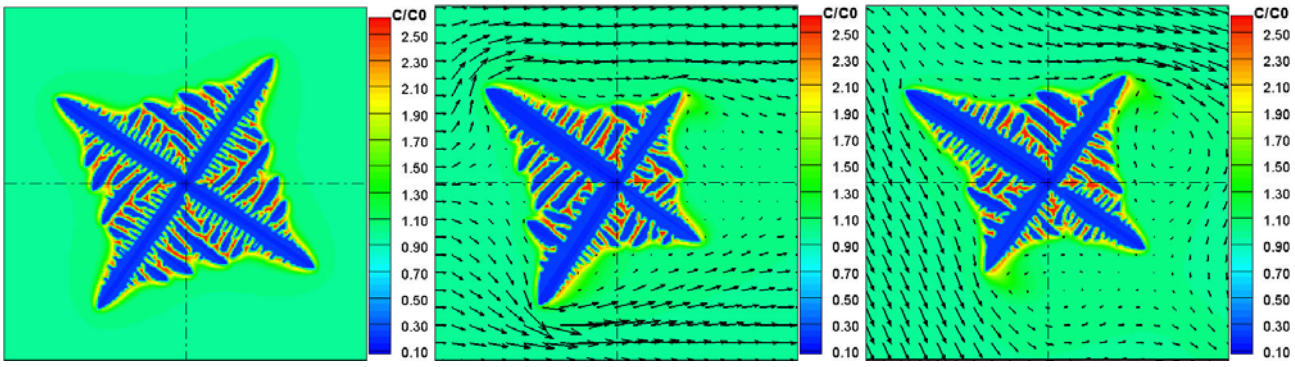

(a) (b) (c)

Figure 3 : Simulated dendritic growth morphology of an Al-2wt%Cu alloy solidified in an undercooled static melt ($\Delta T = 10.5K$) with a preferred growth orientation of $\theta_0 = 65^0$ under various flow directions: (a) no flow(P_e=0), (b) horizontal flow(P_e=0.162) and (c) flow from 45^0($P_e(x) = P_e(y)$=0.115).

Figure 4 shows the variation of the composition and the growth velocity at the dendrite tips with time for the case of Fig. 1 (b). Figure 4(a) indicates the schematics of a dendrite. As shown in Fig.4 (a), the tips growing into the upstream, the dowstream and the perpendicular directions are referred as the upstream tip (ut), the downstream tip (dt) and the perpendicular tip (pt), respectively. It can be seen from Fig. 4(c) that all the tip velocities in the initial stage have a relatively large value. At the initial stage, the local undercooling for dendritic growth includes only the imposed thermal undercooling.

As solidification proceeds, solute atoms are liberated and enriched in the solid/liquid interface, leading to a rapid increase of concentration in front of the dendrite tips as shown in Fig. 4(b). Due to the negative liquidus slop in this alloy, the increasing local concentration at the interface will result in an increase of the negative solutal undercooling, leading to a rapid decrease in the tip growth velocity as shown in Fig. 4(c). After a transient period, the concentration ahead of the upstream tip reaches an approximately stable value. This indicates that the solute rejection is balanced by the solute transportation due to convection and diffusion.

Correspondingly, the upstream tip reaches the steady state growth with a velocity about 50% higher than that for pure diffusion. Meanwhile, the perpendicular arm tip also approaches an approximately steady state growth and the tip growth velocity increases about 10% compared to the case without fluid flow. In the later stage of dendritic growth, the concentrations in fronts of the upstream and the perpendicular tips are found to a little decrease, leading to a slight increase of the tip growth

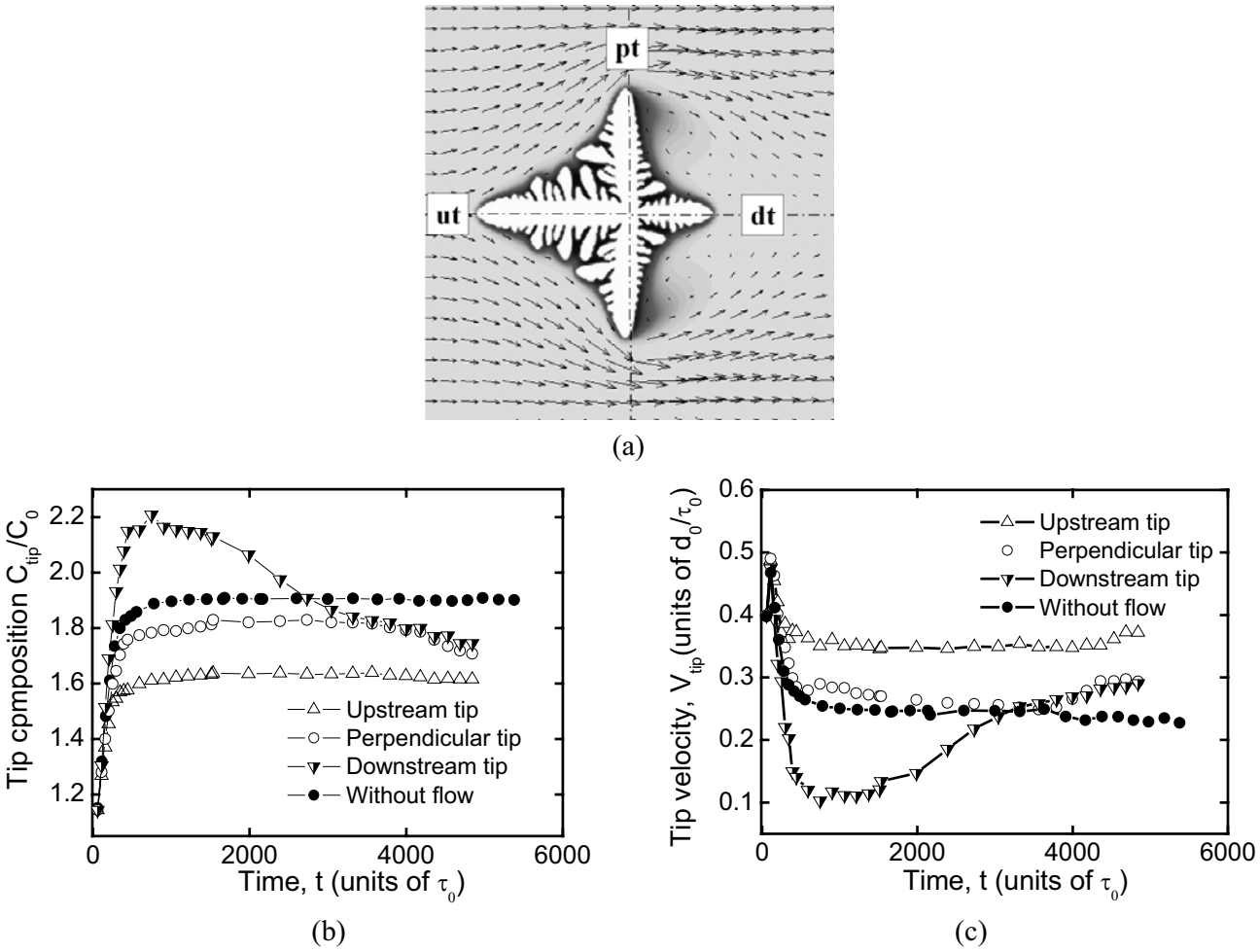

Figure 4 : Variation of the composition and the tip growth velocity at the dendrite tips with time under the condition of $P_e = 0.162$and $\theta_0 = 0^0$: (a) a schematic drawing of a dendrite, (b) tip composition vs. time and (c) tip velocity vs. time.

velocity. This phenomenon is considered to be caused by the increasingly intense impingement of convection against the growing tips when they are close to the side boundaries. On the other hand, the downstream arm exhibits some different growth behavior. As shown in Fig. 4(c), the growth velocity of the downstream tip quickly reaches a minimum which is approximately 50% lower than that for the case without flow, and then gradually increases. This is due to the fact that as a dendrite grows, two clockwise rotating vortices develop in the downstream side. The fluid starts to flow toward the downward growing tip. The local solute is pushed away by the back flow, leading to an increase of the growth velocity of the downstream tip.

3.1.2 Effect of initial alloy composition

The role of the initial alloy composition on dendritic growth morphology under convection was investigated. Figure 5 indicates the simulated dendritic growth morphology and solute profiles with various initial compositions of (a) 1wt%Cu, (b) 2wt%Cu and (c) 4wt%Cu solidified in an undercooled melt with P_e =0.057 andΔT = $12K$. It is apparent that with an increase of solute content, dendrites become finer with enhanced sidebranches. This trend is understandable from the fact that solute addition destabilizes the tip, resulting in a smaller tip radius [Trivedi, Miyahara, Mazumder, Simsek, and Tewari(2001)] and promoting sidebranches. It can also be seen from Fig. 5 that melt flow alters the dendrite shape and the influence of flow is closely related to the

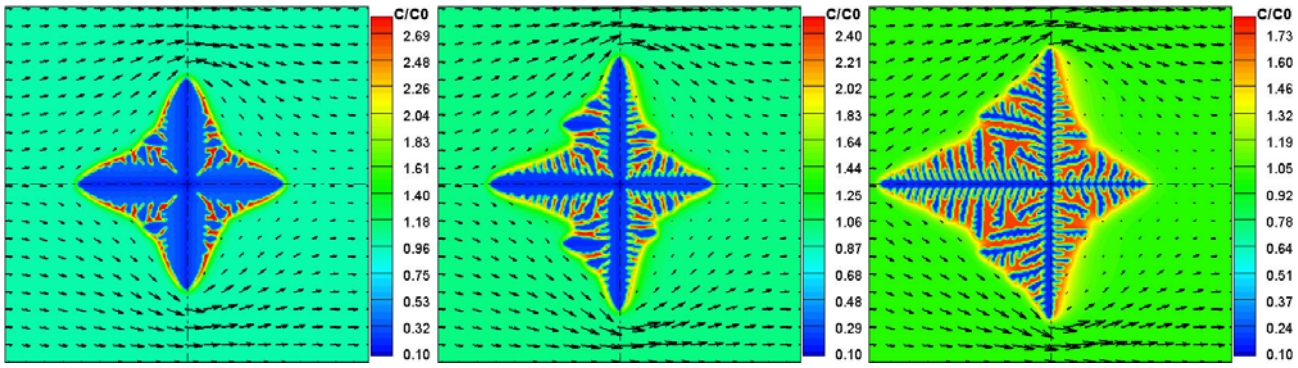

(a) (b) (c)

Figure 5 : Simulated dendritic growth morphology of Al-Cu alloys solidified in a horizontally flowing melt ($P_e = 0.057, \Delta T = 10K$) with various initial compositions: (a) 1wt%Cu, (b) 2wt%Cu and (c) 4wt%Cu.

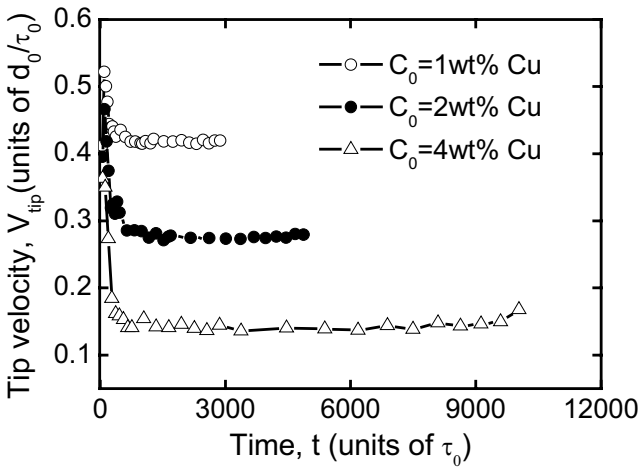

Figure 6 : Effect of initial alloy composition on the tip growth velocity with $\Delta T = 10K$ and an inlet flow velocity of $P_e = 0.057$.

alloy composition. In case of dilute solute content of C_0=1wt%Cu, the dendrite shape seems to be not affected much by the flow. As the solute content increases, the flow effect, i.e. the asymmetric growth features of the convective dendrites, becomes increasingly noticeable as shown in Fig. 5 (a) through (c). The effect of initial alloy composition on tip growth velocity of convective dendrites was also evaluated. Figure 6 represents the growth velocities of the upstream tip with various initial alloy compositions obtained from the simulation of Fig. 5. A general trend can be seen from the figure that after an initial rapid growth, the tip growth velocities for various compositions fall to their steady state levels. Typically, with an increase of solute content, the growth of a dendritic tip in the steady-state propagation region becomes slower. This tendency coincides with the theoretical predictions [Lipton, Glicksman and Kurz(1987)]. From the foregoing analysis, the rejected amount of solute from the growing dendrites increases with an increase of solute content, leading to a larger solute enrichment in the solid/liquid interface. It is understood that a higher local solute enrichment at the interface will give rise to a larger negative solutal undercooling and thereby a smaller dendritic growth velocity.

3.2 Multi-dendritic growth in solidification of ternary alloys

The MCA-transport model was coupled with the thermodynamic and phase equilibrium calculation to simulate the dendritic growth of ternary alloys in the presence of melt convection.

3.2.1 Columnar dendritic growth in directional solidification

Figure 7 indicates the simulated dendritic growth morphology and the composition maps of Cu and Mg, for an Al-3.9wt%Cu-0.9wt%Mg alloy solidified directionally in a static melt. The calculation domain consists of 260×220 cells with a cell size of 2 μm. The temperature field in the entire calculation domain was assumed to be homogeneous with an undercooling of $\Delta T = 12K$. At the beginning of calculation, seven crystal seeds were assigned on the bottom of the calculation domain with a uniform arrangement. The seeds were assumed to have the same crystallographic orientation of $\theta_0 = 0^0$ with respect to the vertical direction. It can be seen from

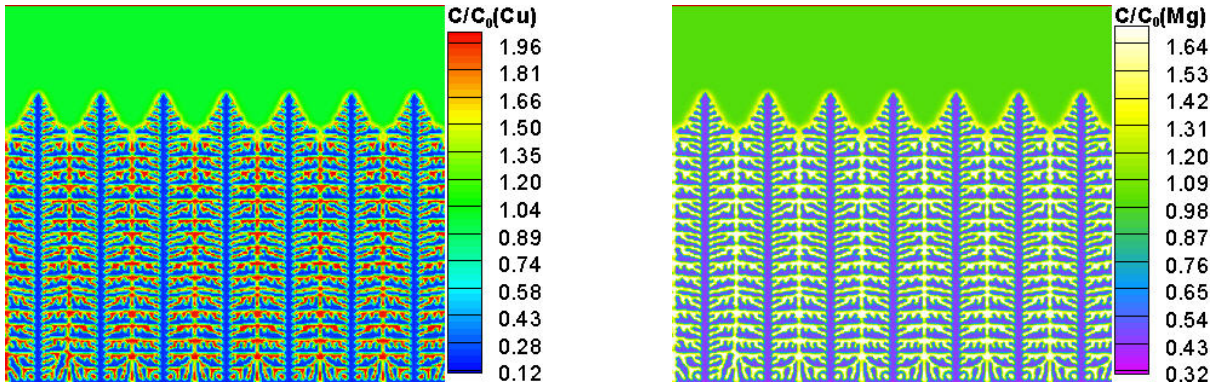

Figure 7 : Simulated columnar dendritic growth morphology and solute fields of (a) Cu and (b) Mg for an Al-3.9wt%Cu-0.9wt%Mg alloy solidified under $P_e = 0$ and $\Delta T = 12K$.

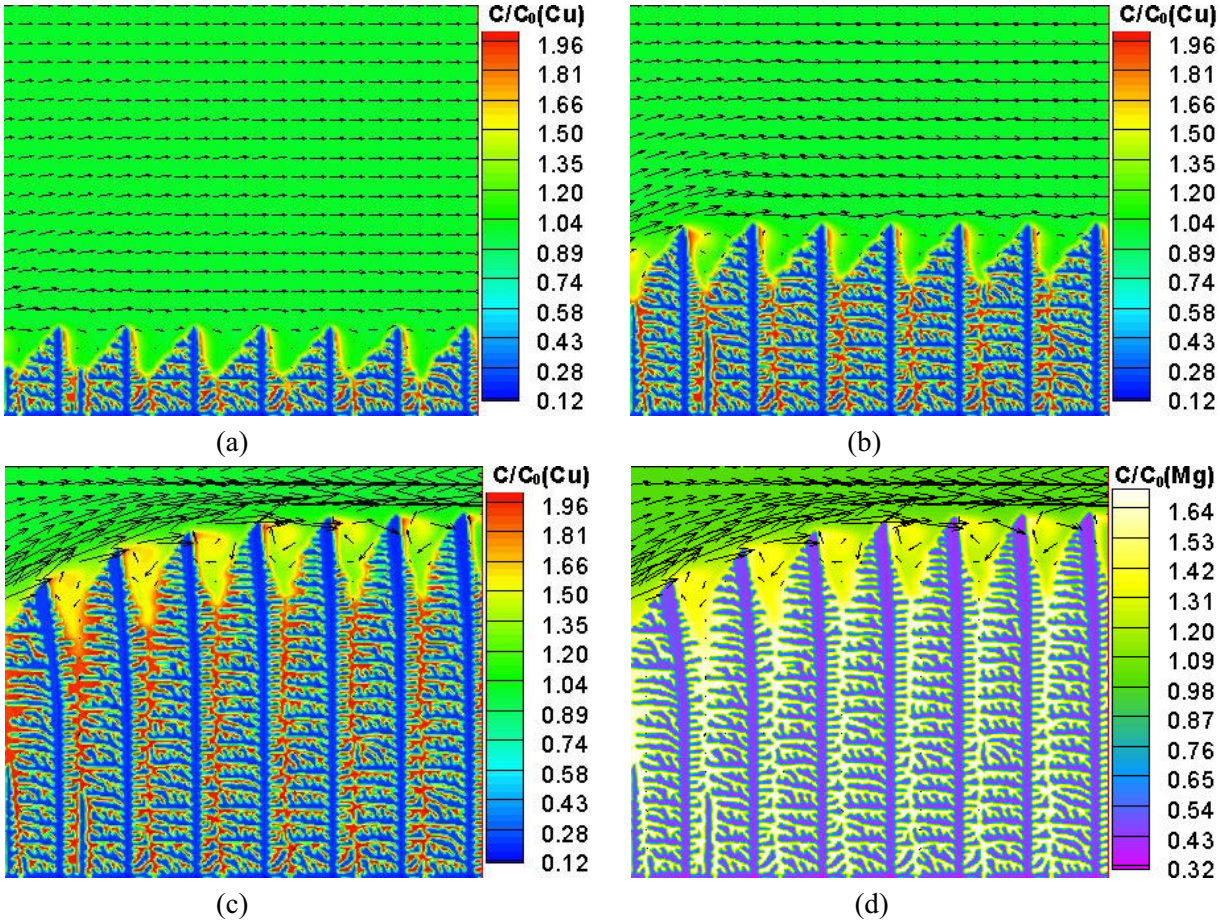

Figure 8 : Simulated columnar dendritic growth morphology, solute profiles and velocity vectors for an Al-3.9wt%Cu-0.9wt%Mg alloy solidified directionally under $P_e = 0.071$ and $\Delta T = 12K$with various elapse times: (a) 2.06×10^4, (b) 4.5×10^4, (c) and (d) 7.88×10^4. Here (a), (b) and (c) show the composition map of Cu, and (d) the composition map of Mg.

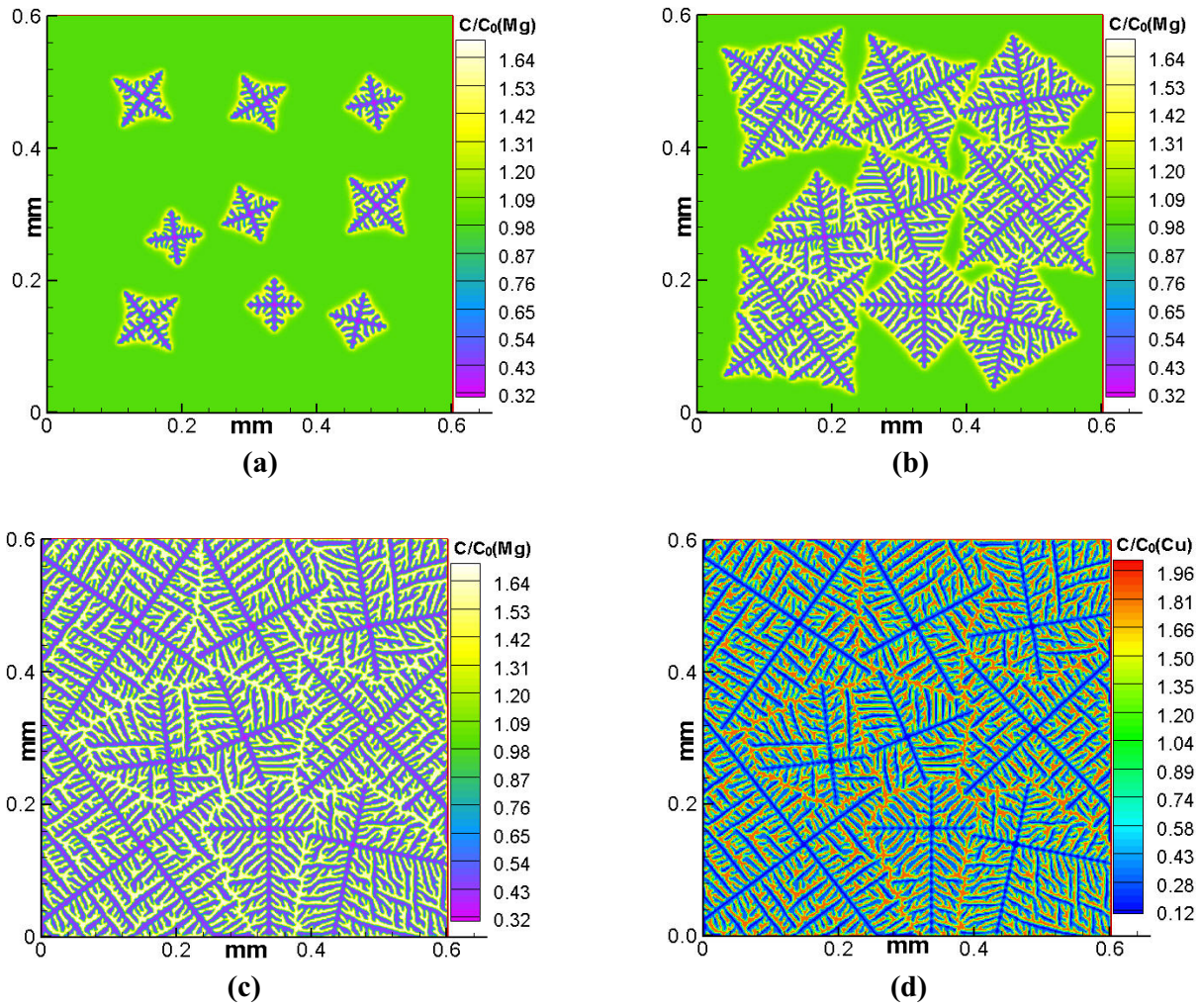

Figure 9 : Simulated evolution of multi-equiaxed dendritic growth for an Al-3.9wt%Cu-0.9wt%Mg alloy solidified in a static melt under $\Delta T = 10K$ with various elapse times: (a) 1.02×10^4 (f_s=0.06), (b) 2.6×10^4 (f_s=0.33), (c) and (d) 4.75×10^4 (f_s=0.6). Here (a), (b) and (c) show the composition map of Mg, and (d) the composition map of Cu.

Fig. 7 that in case without melt convection, a symmetrical solute profile is obtained around the growing dendrites, leading to the symmetrical dendrite morphology with well developed sidebranches.

Figure 8 indicates the simulated dendritic growth morphology and the composition maps of Cu and Mg, for an Al-3.9wt%Cu-0.9wt%Mg alloy solidified directionally with an inlet flow velocity of P_e =0.071 from left to right for various elapse times: (a) 2.06×10^4, (b) 4.5×10^4, (c) and (d) 7.88×10^4. In Fig. 8, (a), (b) and (c) show the composition map of Cu, and (d) the composition map of Mg. Other calculation conditions of Fig. 8 are identical to those of Fig. 7. As shown in the figure, the dendrites solidified directionally with melt flow exhibit asymmetrical growth morphology. Sidebranches are found to be largely favored on the upstream edges of the main stems and suppressed on the other side. Besides, the secondary dendrite arms formed in the upstream region appear to grow a little upwards. It is to be noted that bulk fluid flow moving from left to right distorts significantly the solute profiles around the growing dendrites. The compositions of the two solutes are lower in the liquid around the forehead of the dendrites and higher on the rear side of the main stems, which represses side-branching in the downstream region of the dendrites. Another interesting phenomenon is that the main stems are no longer vertical and obviously deflected into the incoming flow. In addition, as the dendrites grow, the main stems become thicker. It

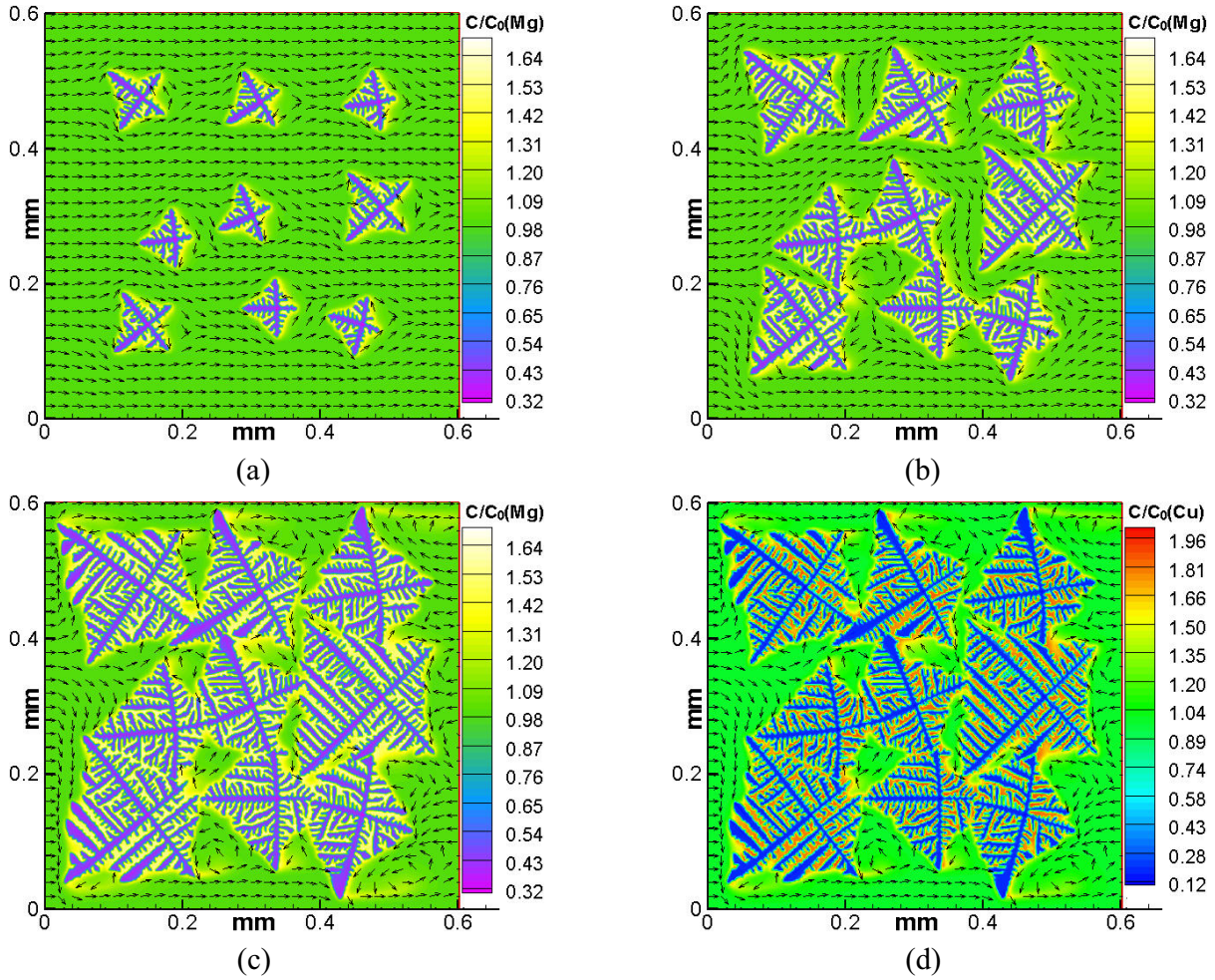

Figure 10 : Simulated evolution of multi-equiaxed dendritic growth for an Al-3.9wt%Cu-0.9wt%Mg alloy solidified in a flowing melt under $P_e = 0.0567$ and $\Delta T = 10K$ with various elapse times: (a) 7.64×10^3 (f_s=0.06), (b) 1.38×10^4 (f_s=0.18), (c) and (d) 1.93×10^4 (f_s=0.33). Here (a), (b) and (c) show the composition map of Mg, and (d) the composition map of Cu.

can also be noted that in the later stage, the flow velocity around the dendrite tips becomes much faster than the early stage due to the impingement of fluid flow against the deflected growing dendrites.

3.2.2 Multi-equiaxed dendritic growth

The present model was also applied to simulate multi-equiaxed dendritic growth in a ternary alloy system. The simulation was carried out in a calculation domain consisting of 300×300 cells with a cell size of $2\mu m$. Nine nuclei are assumed to have randomly given preferred growth orientations ranging from 0° to 90° with respect to the horizontal direction and randomly distributed in the calculation domain.

Figure 9 illustrates the simulated evolution of multi-equiaxed dendritic growth of an Al-3.9wt%Cu-0.9wt%Mg alloy in a static undercooled melt with $\Delta T = 10K$ for various elapse times and solid fractions: (a) 1.02×10^4 (f_s=0.06), (b) 2.6×10^4(f_s=0.33), (c) and (d) 4.75×10^4 (f_s=0.6). In Fig. 9, (a), (b) and (c) indicate the composition map of Mg, and (d) the composition map of Cu. It can be seen that in the early stage of solidification, the main arms of the equiaxed dendrites grow along their crystallographic orientations, together with the branching of secondary arms.

As the solidification proceeds, the equiaxed dendrites collides each other and the morphology is affected thereby. Finally, the dendrites impinge on each other to

form grain boundaries.

Figure 10 illustrates the evolution of multi-dendritic growth of an Al-3.9wt%Cu-0.9wt%Mg alloy with a horizontal flow of P_e =0.0567 for various elapse times and solid fractions: (a) 7.64×10^3 (f_s=0.06), (b) 1.38×10^4 (f_s=0.18), (c) and (d) 1.93×10^4 (f_s=0.33). Other conditions for the simulation of Fig. 10 are the same as those of Fig. 9. The flow field in Fig. 10 is plotted using the uniform vectors. Comparing Fig. 10 with Fig. 9, it is shown that completely different dendritic growth patterns can be obtained in the presence of melt flow. Dendritic growth is always enhanced in the upstream direction and inhibited in the downstream direction. The primary and secondary arms are distinctly deflected in the upstream direction. The dendrite arms in the upstream region are obviously coarser than those growing from a static melt. Moreover, comparing Fig. 10 (a) with Fig. 9 (a) and Fig. 10 (c) with Fig. 9 (b), it can be seen that the times to reach the same solid fraction with melt convection become shorter than those without melt convection. This is due to the fact that fluid flow promotes solute transport in the melt, and thus hastens the overall solidification process. It is to be noted that at the early stage of solidification, melt flows from left to right more or less smoothly along the small dendrites and solute is transported from the upstream region to the downstream region of each dendrite, resulting in lower growth velocity and fewer sidebranches in the downstream region. As the dendritic growth continues, dendrites collides each other, leading to the change of flow direction in the inner region. At the later stage, the flow becomes very complex and some rotating vortices appear in the inter-dendritic flow region.

4 Conclusions

The solutally driven dendritic growth behavior of binary and ternary Al-rich alloys in the presence of fluid flow has been simulated based on a two-dimensional modified cellular automaton (MCA)-transport model. In the present model, the cellular automaton algorithm is fully coupled with the numerical solution of momentum and species transport equations. Coupled with a thermodynamic and phase equilibrium calculation, the model was extended to a multi-component alloy system and applied to simulate the multi-dendritic growth morphology of an Al-Cu-Mg ternary alloy in the presence of fluid flow. The results are summarized as follows.

1. The simulation results reveal that melt convection significantly affects dendritic growth behavior, and that the tip velocity is enhanced in the upstream and inhibited in the downstream regions, respectively.

2. The dendritic growth is remarkably influenced by the flow direction. Quite different dendrite shapes and tip growth velocities are obtained with different flow directions even though other solidification conditions are exactly identical.

3. Alloy composition is found to play an important role on the growth of convective dendrites. With an increase of solute content, the effect of melt convection on dendritic growth becomes increasingly stronger.

4. Coupling of the MCA model with a thermodynamic and phase equilibrium calculation enables to extend the present model to be applied to multi-component system.

5. Based on the simulation of columnar dendritic growth in directional solidification of an Al rich ternary alloy, convection was found to promote not only the deflection of the primary arms, but also the side-branching of secondary arms in the direction of the incoming flow, leading to asymmetrical dendritic growth.

6. In multi-equiaxed dendritic growth of an Al rich ternary alloy under convection, dendritic growth was also found to be enhanced in the upstream direction and inhibited in the downstream direction.

Acknowledgement: We wish to thank Professor Y. Austin Chang at the University of Wisconsin-Madison, USA, for kindly providing PanEngine. We also thank Dr. S. -L. Chen, Mr. W. Cao and Mr. T. Dai for their help in coupling PanEngine with MCA. The research of M.F.Z. was supported by the National Natural Science Foundation of China (Grant Nos. 50371015 and 50471025).

References

Al-Rawahi, N.; Tryggvason, G. J. (2002): Numerical simulation of dendritic solidification with convection: two dimensional geometry. *Comp. Phys.*, vol. 180, pp. 471-496.

Amberg, G.; Shiomi, J.(2005): Thermocapillary flow and phase change in some widespread materials processes, *FDMP: Fluid Dynamics & Materials Processing,* vol. 1, no.1, pp.81-95.

Belteran-Sanchez, L.; Stefanescu, D. M. (2004): A qantitative dendrite growth model and analysis of stability concepts. *Metall Mater Trans A*, vol. 35, pp. 2471-2485.

Chen, S-L.; Daniel, S.; Zhang, F.; Chang, Y. A.; Yan, X-Y; Xie, F-Y; Schmid-Fetzer, R.; Oates, W. A. (2002): The PANDAT software package and its applications. *CALPHAD*, vol. 26(2), pp. 175-188.

Hong, C. P. (2004): Computer modeling of heat and fluid flow in materials processing, *IOP Publishing Ltd.*, Bristol and Philadelphia.

Jeong, J. H.; Dantzig, J. A.; Goldenfeld, N. (2003): Dendritic growth with fluid flow in pure materials. *Metall and Mater Trans A*, vol. 34A, pp. 459-466.

Kim, S. G.; Kim, W. T.; Suzuki, T. (1999): Phase-field models for binary alloys. *Phys Rev E*, vol. 60, pp. 7186-7197.

Koss, M. B.; LaCombe, J. C.; Tennenhouse, L. A.; Glicksman, M. E.; Winsa, E. A. (1999): Dendritic growth tip velocities and radii of curvature in microgravity. *Metall and Mater Trans. A*, vol. 30A, pp. 3177-3190.

Lan, C. W.; Shih, C. J. (2004): Efficient phase field simulation of a binary dendritic growth in a forced flow. *Phys Rev E*, vol. 69, 031601.

Lappa, M.(2005): Coalescence and non-coalescence phenomena in multi-material problems and dispersed multiphase flows: Part 1, A critical review of theories, *FDMP: Fluid Dynamics & Materials Processing,* vol. 1, no.3, pp.201-211.

Lappa, M.(2005): Coalescence and Non-coalescence phenomena in multi-material problems and dispersed multiphase flows: Part 2, A critical review of CFD approaches, *FDMP: Fluid Dynamics & Materials Processing,* vol. 1, no.3, pp.213-234.

Lee, Y. C.; Chen, F. (1995): Volume change effect on the salt-finger stability of directionally solidifying ammonium chloride solution. *J Cryst Growth*, vol. 154, pp. 351-363.

Lijian, Tan; Nicholas, Zabaras (2006): A level set simulation of dendritic solidification with combined features of front-tracking and fixed-domain methods. *J. Comp. Phys.*, vol. 211, pp. 36-63.

Lipton, J.; Glicksman, M. E.; Kurz, W. (1987): Equiaxed dendrite growth in alloys at small supercooling. *Metall Trans*, vol. 18A, pp. 341-345.

Murray, B. T.; Wheeler, A. A.; Glicksman, M. E. (1995): Simulation of experimentally observed dendritic growth behavior using a phase-field model. *J. Cryst. Growth*, vol. 154, pp. 386-400.

Nastac, L. (1999): Numerical modeling of solidification morphologies and segregation patterns in cast dendritic alloys. *Acta Mater*, vol. 47, pp. 4253-4262.

Natsume, Y.; Ohsasa, K.; Narita, T. (2002): Investigation of the mechanism of alloy dendrite deflection due to flowing melt by phase-field simulation. *Mater Trans*, vol. 43, pp. 2228-2234.

Patankar, S. V. (1980): Numerical heat transfer and fluid flow, *Hemisphere Pub. Corp.*, New York.

Saville, D. A.; Beaghton, P. J. (1988): Growth of needle-shaped crystals in the presence of convection. *Phys Rev A*, vol. 37, pp. 3423-3430.

Schraga, D.S. (1999): A simplified model of dendritic growth in the presence of natural convection. *J Cryst Growth*, vol. 205, pp. 410-426.

Shin, Y. H.; Hong, C. P. (2002): Modeling of dendritic growth with convection using a modified cellular automaton model with diffuse interface. *ISIJ Int.*, vol. 42, pp. 359-367.

Thomas, L.H. (1949): Elliptic problems in linear difference equations over a network. *Sci. Comp. Lab. Rept.*, Columbia University, New York.

Tong, X; Beckermann, C; Karma, A; Li, Q. (2001): Phase-field simulations of dendritic crystal growth in a forced flow. *Phys Rev E*, vol. 63, pp. 061601.

Trivedi, R.; Miyahara, H.; Mazumder, P.; Simsek, E.; Tewari, S. N. (2001): Directional solidification microstructure in diffusive and convective regimes. *J Cryst Growth*, vol. 222, pp. 365-379.

Udaykumar, H. S.; Marella, S; Krishnan, S. (2003): Sharp-interface simulation of dendritic growth with convection: benchmarks. *Int. J Heat and Mass Transfer*, vol. 46, pp. 2615-2627.

Wheeler, A. A.; Boettinger, W. J.; McFadden, G. B. (1992): Phase-field model for isothermal phase transitions in binary alloys. *Phys Rev A*, vol. 45, pp. 7424-7439.

Zhu, M. F.; Cao, W.; Chen, S.-L.; Hong, C.P.; Chang, Y. A. (2006): Modeling of Microstructure and microsegregation in solidification of multi-component alloys. *J. of Phase Equilibrium and Diffusion*, (accepted).

Zhu, M. F.; Dai, Ting; Lee, S. Y.; Hong, C. P. (2005): Modeling of dendritic Growth in the Presence of Convection. *Science in China*, vol. 48(3), pp. 241-257.

Zhu, M. F.; Hong, C. P. (2001): A modified cellular automaton model for the simulation of dendritic growth in solidification of alloys. *ISIJ Int.*, vol. 41, pp. 436-445.

Zhu, M. F.; Hong, C. P. (2002): Modeling of microstructure evolution in regular eutectic growth. *Phys Rev B*, vol. 66, 155428.

Zhu, M. F.; Hong, C. P. (2004): Modeling of irregular eutectic microstructures in solidification of Al-Si alloys. *Metal.Mater. Trans. A,* vol. 35, pp. 1555-1563.

Zhu, M. F.; Hong, C. P.;Stefanscu, D.M.; Chang, Y.A. (2006): Computational modeling of microstructure evolution in solidification of Al alloys. *Metal.Mater. Trans. B,* (in press)

Zhu, M. F.; Lee, S. Y.; Hong, C. P. (2004): Modified cellular automaton model for the prediction of dendritic growth with melt convection. *Phys Rev E*, vol. 69, 061610.